Supplement of Atmos. Chem. Phys., 17, 2509–2523, 2017
http://www.atmos-chem-phys.net/17/2509/2017/
doi:10.5194/acp-17-2509-2017-supplement


Atmospheric Chemistry and Physics Open Access EGU

*Supplement of*

# Aerosol vertical distribution and optical properties over China from long-term satellite and ground-based remote sensing

**Pengfei Tian et al.**

*Correspondence to:* Lei Zhang (zhanglei@lzu.edu.cn) and Renyi Zhang (renyi-zhang@tamu.edu)

**Table S1.** Basic information of the selected AERONET sites over China

| Region | Site Number | Site name | Longitude (° N) | Latitude (° E) | Altitude (m) | AOD points | Inversion points |
|---|---|---|---|---|---|---|---|
| LP | 1 | Jingtai | 104.100 | 37.333 | 1604 | 1435 | 66 |
| | 2 | Lanzhou_City | 103.853 | 36.048 | 1516 | 1231 | 117 |
| | 3 | SACOL | 104.137 | 35.946 | 1965 | 50020 | 1552 |
| | 4 | Yulin | 109.717 | 38.283 | 1080 | 6213 | 241 |
| NCP | 5 | Beijing | 116.381 | 39.977 | 92 | 83304 | 3812 |
| | 6 | XiangHe | 116.962 | 39.754 | 36 | 84158 | 3642 |
| | 7 | Xinglong | 117.578 | 40.396 | 970 | 26291 | 543 |
| | 8 | Yufa_PEK | 116.184 | 39.309 | 20 | 400 | 39 |
| PRD | 9 | Hong_Kong_Hok_Tsui | 114.258 | 22.210 | 80 | 4189 | 201 |
| | 10 | Hong_Kong_PolyU | 114.180 | 22.303 | 30 | 23796 | 335 |
| | 11 | Hong_Kong_Sheung | 114.117 | 22.483 | 40 | 2471 | 82 |
| | 12 | Zhongshan_Univ | 113.390 | 23.060 | 27 | 1259 | 64 |
| TP | 13 | NAM_CO | 90.962 | 30.773 | 4740 | 15502 | 8 |
| YRD | 14 | Hangzhou-ZFU | 119.727 | 30.257 | 14 | 888 | 64 |
| | 15 | Hefei | 117.162 | 31.905 | 36 | 2534 | 196 |
| | 16 | Shouxian | 116.782 | 32.558 | 22 | 2027 | 223 |
| | 17 | Taihu | 120.215 | 31.421 | 20 | 22344 | 1989 |
| Desert | 18 | Dunhuang | 94.794 | 40.038 | 1300 | 557 | 8 |
| | 19 | Dunhuang_LZU | 94.955 | 40.492 | 1061 | 832 | 8 |
| | 20 | Minqin | 102.959 | 38.607 | 1373 | 699 | 4 |
| | 21 | Zhangye | 100.276 | 39.079 | 1461 | 1818 | 20 |

**Table S2** Main technical parameters of the CALIOP and NIES lidar

| **Parameter** | **CALIOP** | **NIES lidar** |
|---|---|---|
| Transmitter | Nd:YAG | Nd:YAG |
| Wavelength (nm) | 532 nm,1064 nm | 532 nm, 1064 nm |
| Pulse Repetition Frequency (Hz) | 20.25Hz | 10 Hz |
| Output Power (mJ) | 110 | 20 |
| Pulse Width (ns) | 20 | 10 |
| Filter Bandwidth (nm) | 0.77(532 nm)<br>0.45 (1064nm) | 3 |
| Telescope | Cassegrainian | Cassegrainian |
| Receiver Telescope Diameter (mm) | 1000 | 200 |
| Field of View (μrad) | 130 | 1000 |
| Detector | APD (1064 nm)<br>PMT (532 nm) | APD (1064 nm)<br>PMT (532 nm) |
| Time Resolution (min) | -- | 15 |
| Vertical Resolution (m) | 30, 60 | 6 |

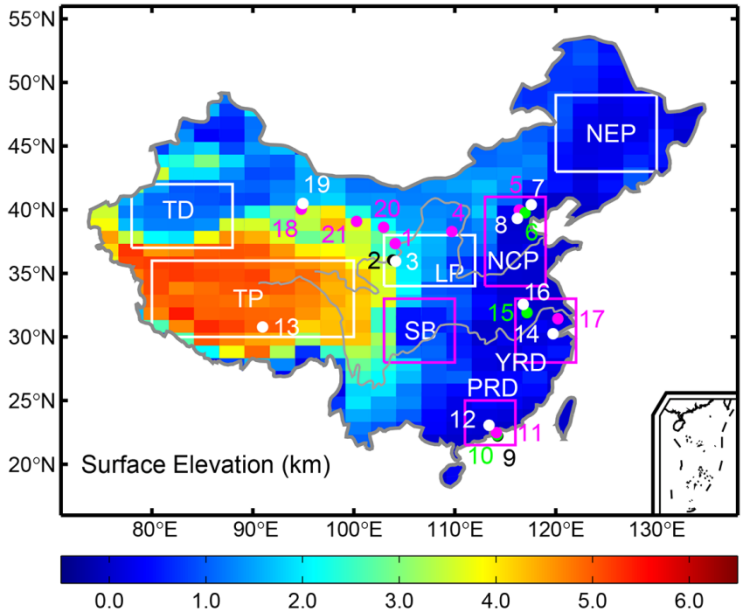


**Figure S1.** Locations (filled circles) of the selected AERONET sites over China. The site numbers are the same as in Table S1.

5

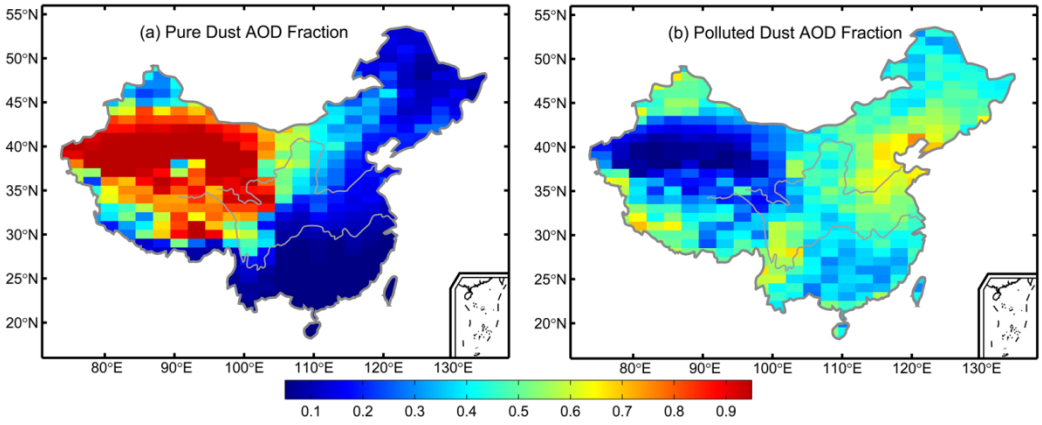


**Figure S2.** Annual pure dust and polluted dust AOD to total AOD ratio over China derived from CALIOP observations from June 2006 to January 2016, with a 1.0°×2.5° latitude-longitude grid.

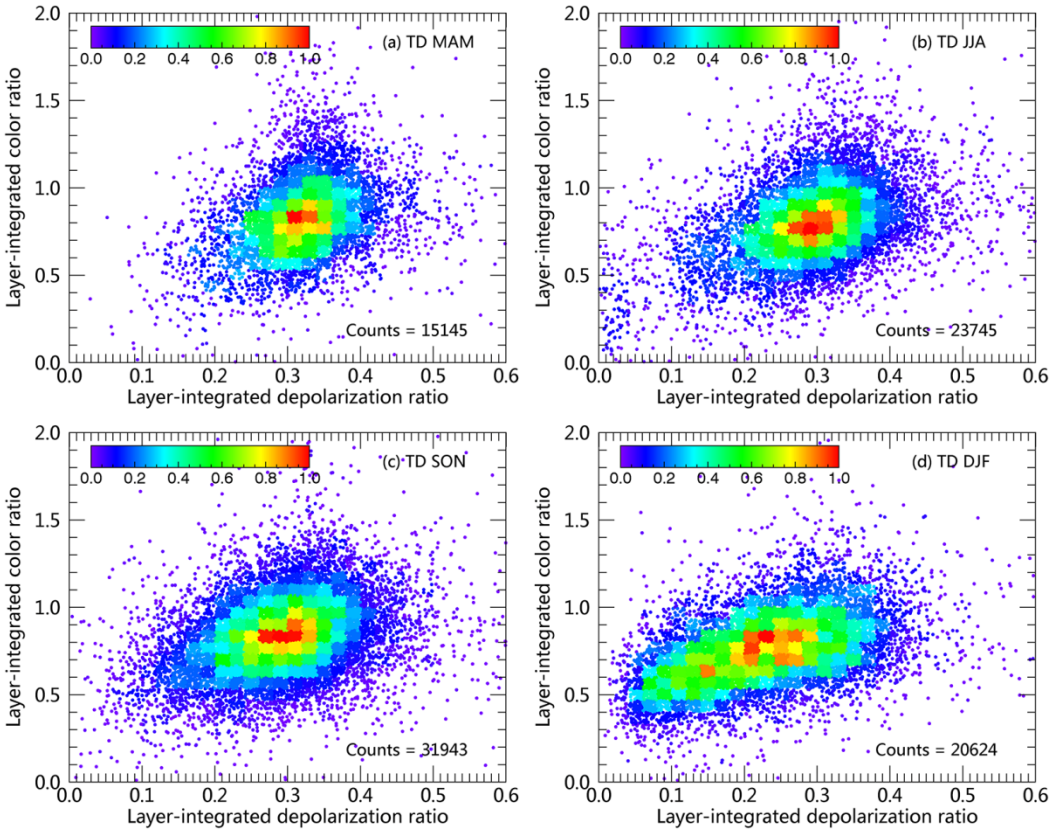


**Figure S3:** Scatter plots for the layer-integrated aerosol color ratios versus the layer-integrated aerosol depolarization ratios over the Taklimakan Desert (TD) region (a) spring, (b) summer, (c) autumn, and (d) winter.

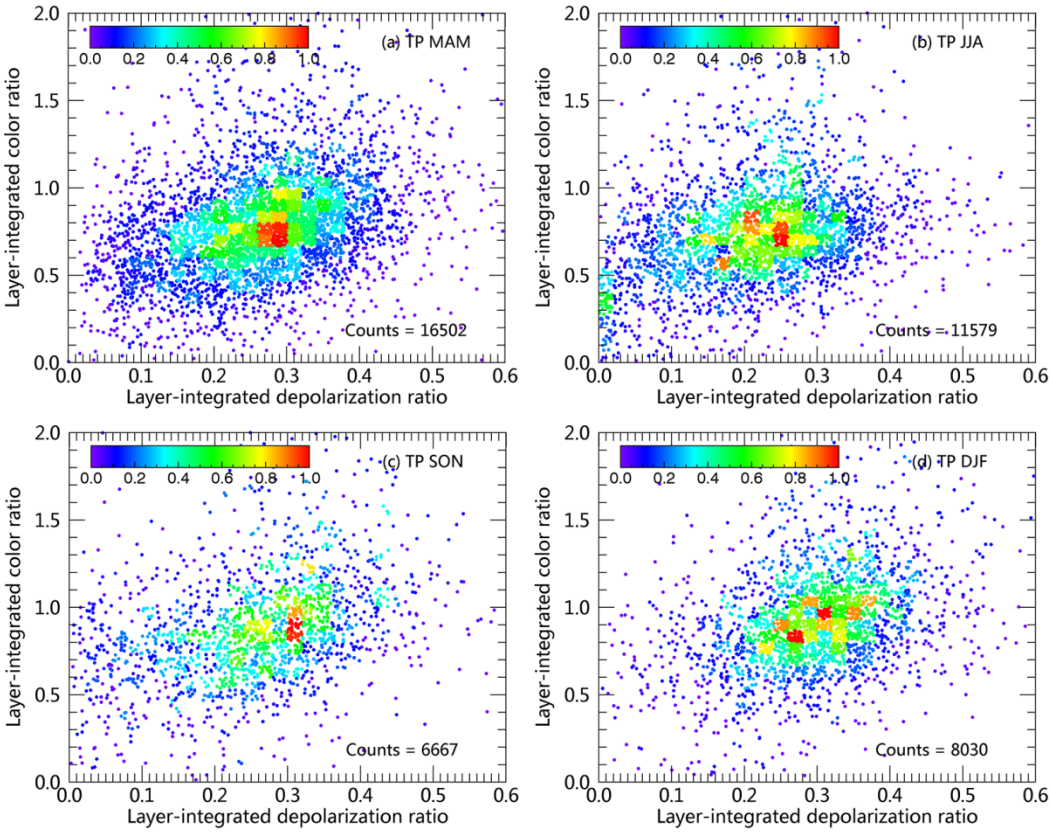


**Figure S4:** Scatter plots for the layer-integrated aerosol color ratios versus the layer-integrated aerosol depolarization ratios over the Tibetan Plateau (TP) region (a) spring, (b) summer, (c) autumn, and (d) winter.

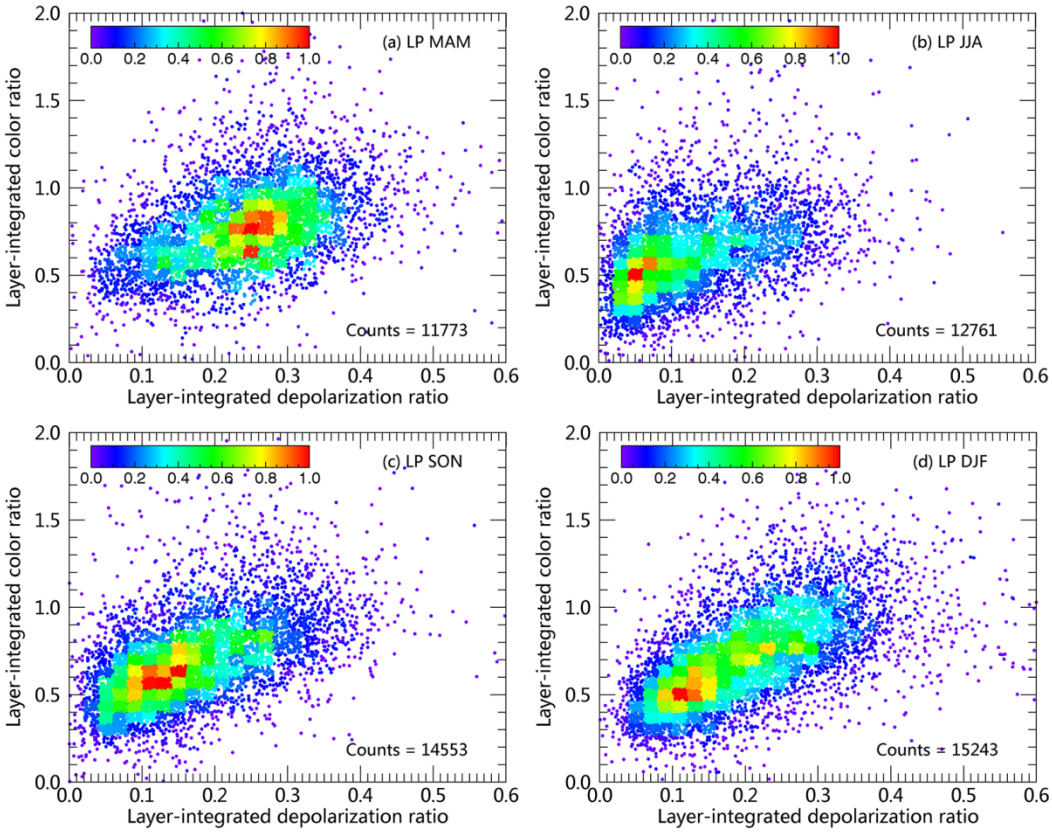


**Figure S5:** Scatter plots for the layer-integrated aerosol color ratios versus the layer-integrated aerosol depolarization ratios over the Loess Plateau (LP) region (a) spring, (b) summer, (c) autumn, and (d) winter.

5

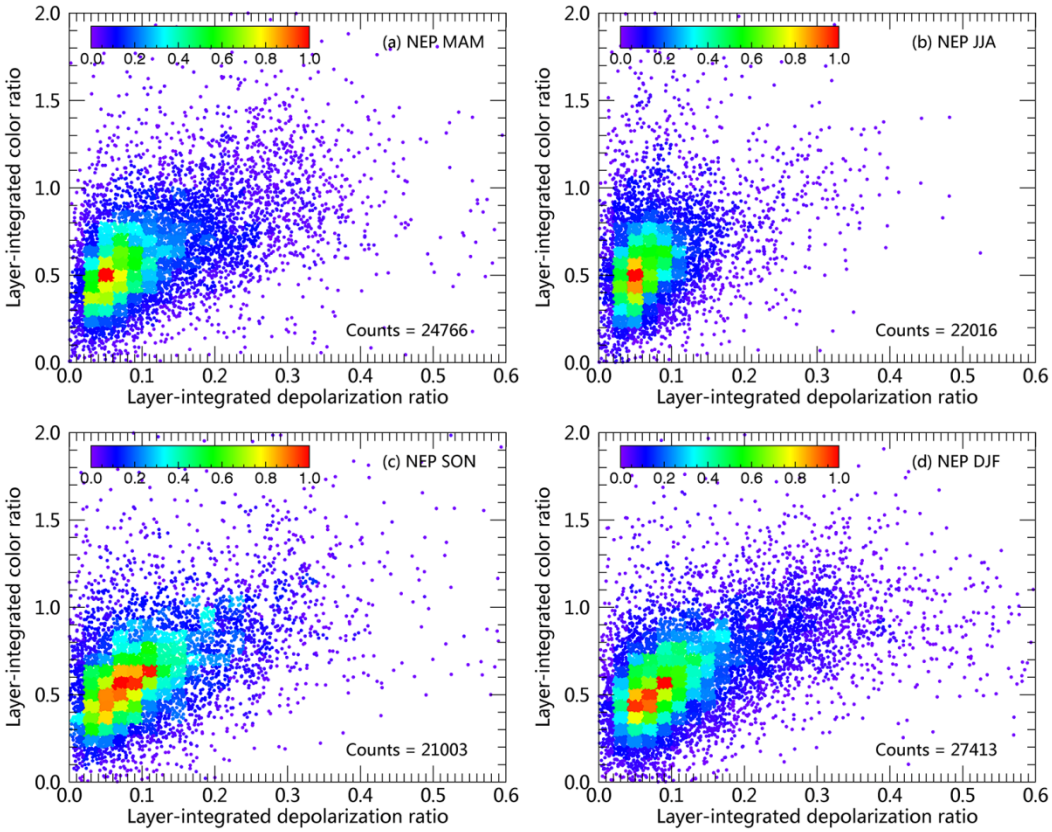


**Figure S6:** Scatter plots for the layer-integrated aerosol color ratios versus the layer-integrated aerosol depolarization ratios over the Northeast China Plain (NEP) region (a) spring, (b) summer, (c) autumn, and (d) winter.

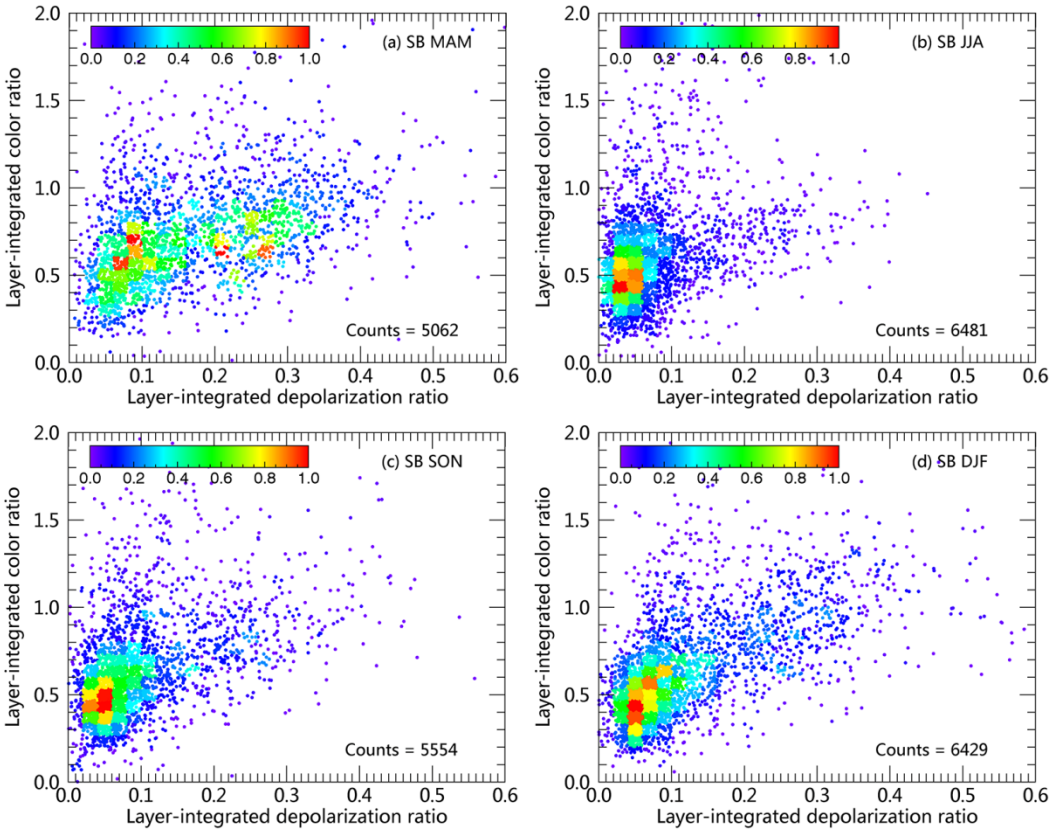


**Figure S7:** Scatter plots for the layer-integrated aerosol color ratios versus the layer-integrated aerosol depolarization ratios over the Sichuan Basin (SB) region (a) spring, (b) summer, (c) autumn, and (d) winter.

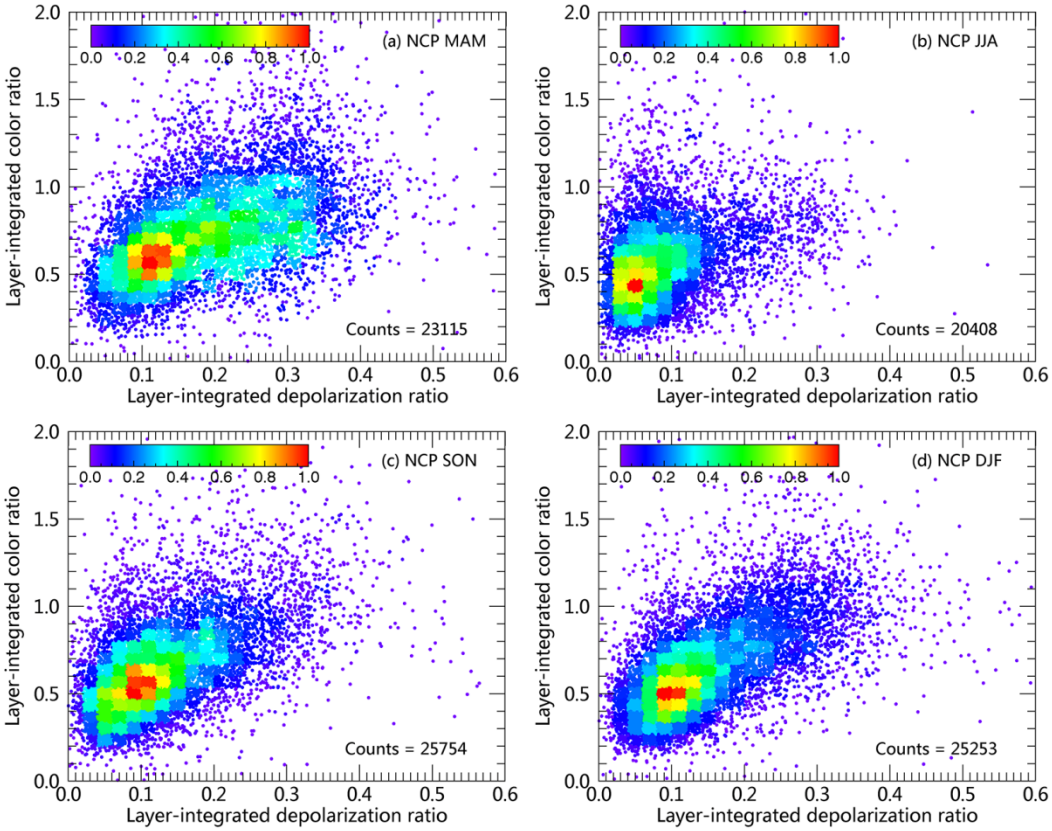


**Figure S8:** Scatter plots for the layer-integrated aerosol color ratios versus the layer-integrated aerosol depolarization ratios over the North China Plain (NCP) region (a) spring, (b) summer, (c) autumn, and (d) winter.

5

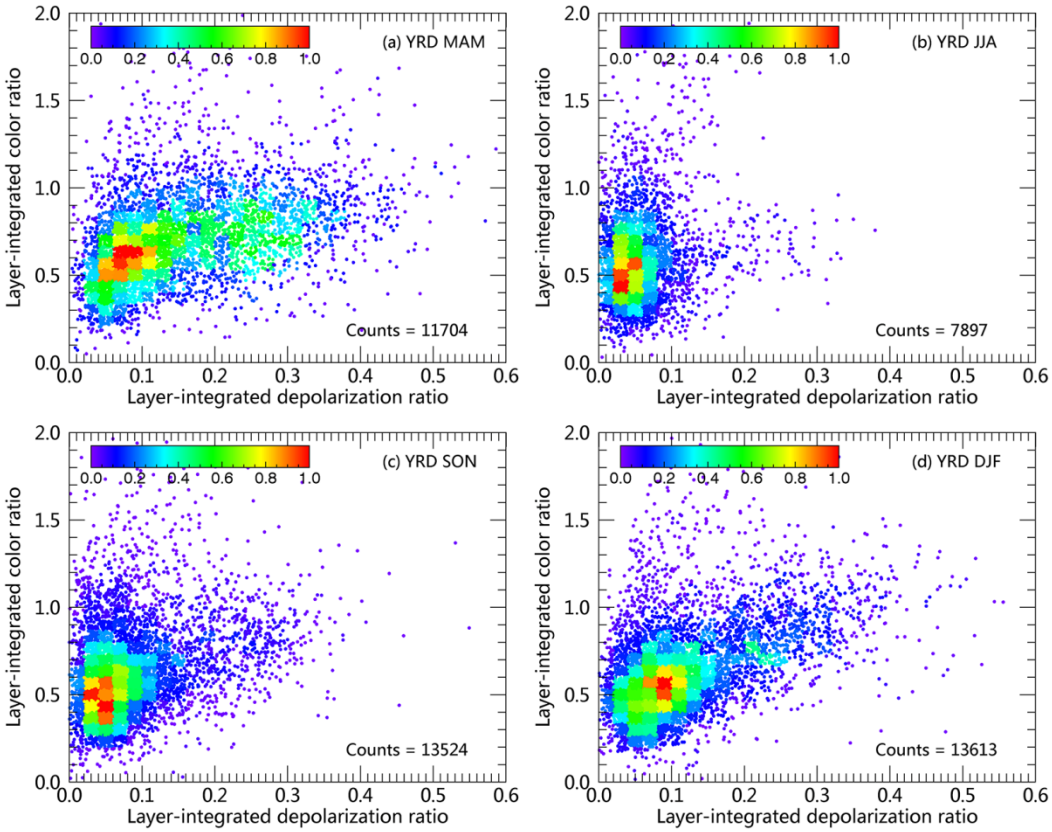


**Figure S9:** Scatter plots for the layer-integrated aerosol color ratios versus the layer-integrated aerosol depolarization ratios over the Yangtze River Delta (YRD) region (a) spring, (b) summer, (c) autumn, and (d) winter.

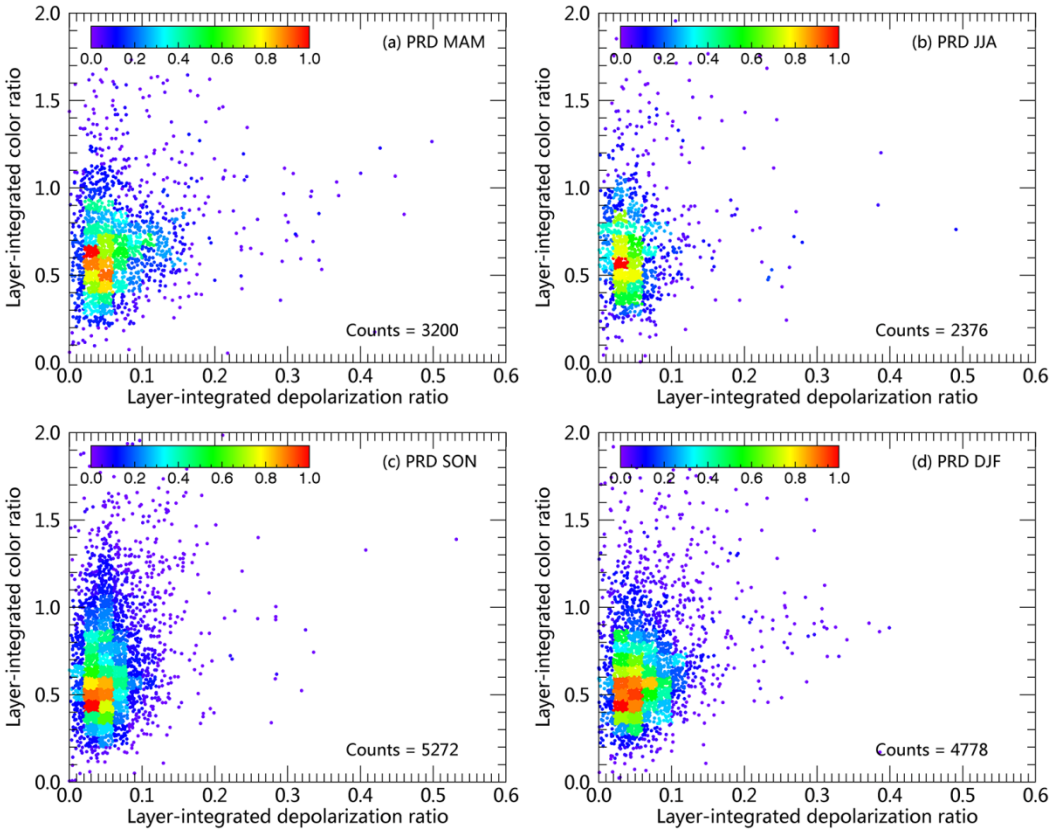


**Figure S10:** Scatter plots for the layer-integrated aerosol color ratios versus the layer-integrated aerosol depolarization ratios over the Pearl River Delta (PRD) region (a) spring, (b) summer, (c) autumn, and (d) winter.

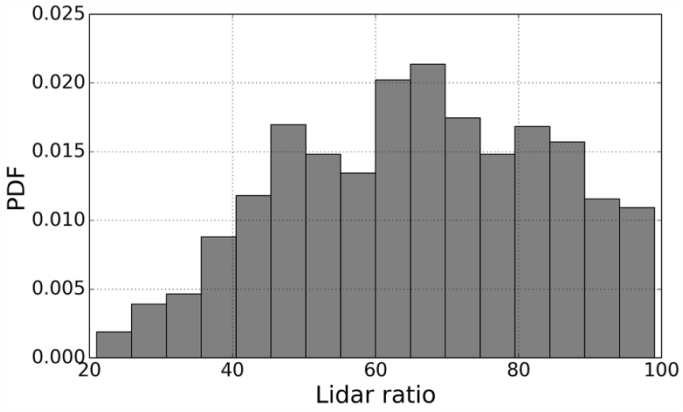


**Figure S11.** Normalized histogram (probability density function, PDF) of the NIES lidar derived lidar ratio.

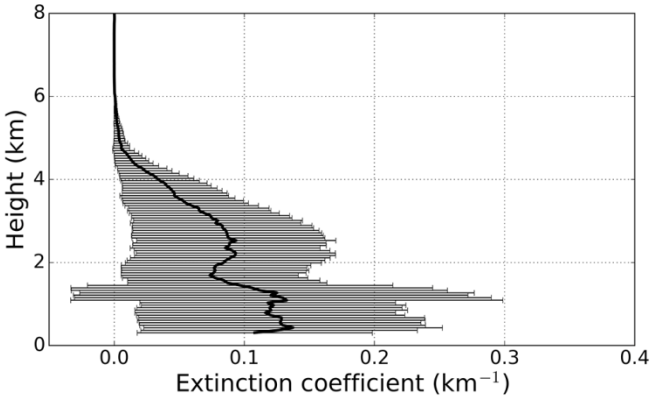


**Figure S12.** Average extinction profile with error bars in the PRD region in spring. The value of the error bar is the average of the extinction coefficient uncertainty in CALIOP Level 2 data product.